Supplementary Information (SI) for Materials Chemistry Frontiers.
This journal is © the Partner Organisations 2025

ELECTRONIC SUPPLEMENTARY MATERIAL

Blue, Green, Yellow and Red Carbon Dots: Confined Synthesis and Mechanism Study

Chao Li,[§a] Yu-quan Zhu,[§b] Xiayan Shao,[a] Kai Song,[c] Wenyan Liu,[a] Kaitao Li,[a] Shanyue Guan,[c] Wendi Liu,[a] and Yanjun Lin*[ade]*

[a] State Key Laboratory of Chemical Resource Engineering, Beijing University of Chemical Technology, Beijing 100029, P. R. China.

[b] Hubei Key Laboratory of Pollutant Analysis & Reuse Technology, College of Chemistry and Chemical Engineering, Hubei Normal University, Huangshi 435002, China.

[c] Key Laboratory of Photochemical Conversion and Optoelectronic Materials, Technical Institute of Physics and Chemistry, Chinese Academy of Sciences, Beijing, 100190, P. R. China.

[d] Salt Lake Chemical Engineering Research Complex, Qinghai Provincial Key Laboratory of Salt Lake Materials Chemical Engineering, Qinghai University, Xining 810016, China.

[e] Quzhou Institute for Innovation in Resource Chemical Engineering, Quzhou 324000, China.

[§] These authors contributed equally to this work.

Experimental Section

Cyclic Voltammetry of CDs

To estimate the HOMO and LUMO energy levels of CDs, the cyclic voltammetry was performed using a three-electrode system. The counter electrode was platinum wire, and the reference electrode was Ag/AgCl. The working electrode was prepared by drop-casting 10 μL of CDs solution (10 mg/mL) onto a platinum electrode followed by drying at 40 °C. The electrolyte was 0.1 M tetrabutylammonium hexafluorophosphate (TBAPF6, Aldrich) in acetonitrile and was purged with N_2 for 20 min prior to use.

The HOMO and LUMO energy levels of CDs were calculated according to the following equations:

$$E_{(HOMO)}=-e(E_{ox}+4.4)\ (Ev) \qquad (1)$$

$$E_{(LUMO)}=-e(E_{red}+4.4)\ (Ev) \qquad (2)$$

Where Eox and Ered are the onset of oxidation and reduction potential, respectively.

Model construction

The models of bulk Mg_3Al-LDH and Mg_2Al-LDH were built according to the experimental X-ray diffraction pattern. The space group of these LDHs was $P-3m1$, with lattice parameters of $\alpha = \beta = 90°$, $\gamma = 120°$.[S1] And the other three lattice parameters (a, b, and c), which were referred to the experimental powder X-ray data, for Mg_3Al-LDH are $a = b = 3.04$ Å, $c = 27.10$ Å, and for Mg_2Al-LDH are $a = b = 3.04$ Å, $c = 25.07$ Å. The $C_6H_4N_2O_3S^-$ (DBS) and $C_{12}H_{25}O_4S^-$ (DS) anions with the

molar ratio of 1:1 were intercalated into the interlayer of the Mg_3Al-LDH and Mg_2Al-LDH to keep the model neutral, and the appropriate amount of water molecules were also added. The chemical formulae for Mg_3Al-LDH and Mg_2Al-LDH are $Mg_{18}Al_6(OH)_{48}(C_6H_4N_2O_3S^-)_3(C_{12}H_{25}O_4S^-)_3 \cdot 78H_2O$ and $Mg_{16}Al_8(OH)_{48}(C_6H_4N_2O_3S^-)_4(C_{12}H_{25}O_4S^-)_4 \cdot 78H_2O$, respectively. And the explicit solvent model of water with a density of 1.0 g/cm^3 was also constructed.

Computational methods

Molecular dynamics (MD) simulations were performed through the Forcite module in Accelrys Materials Studio software package version 5.5. The canonical (NVT) ensemble was selected to guarantee the constant volume system exchanging the heat with the environment at the constant temperature. The universal force field was selected to describe the properties and interactions of atoms. The temperature was set as 298 K controlled by the Nosé thermostat. The Ewald summation method was applied in dealing with the long-range Coulombic interactions and van der Waals interactions.[S2] And the time step was set to be 1 fs and the total dynamics time was 10 ns.

Characterizations

X-ray diffraction patterns (XRD) were obtained by the Bruker D8 diffractometer using a Cu Kα source, with a scan step of 0.02°, a scan rate of 1°/min, and a scan range between 0.5° and 15°. The UV-vis absorption spectra were obtained in the 220–800 nm range using the Shimadzu UV-3600 spectrophotometer, with a slit width of 1.0 nm. The elemental contents of Mg and Al in the samples were determined by inductively coupled plasma-atomic emission spectroscopy (ICP-AES) using the Shimadzu ICPS-7500 instrument. The organic elemental analysis was carried out by the PerkinElmer Elementarvario elemental analysis instrument. The morphology was investigated using a scanning

electron microscope (SEM Hitachi S-3500 N), and the applied accelerating voltage was 20 kV. The TEM images were obtained using the JEOL JEM-2100 transmission electron microscope with the accelerating voltage of 200 kV. The thickness data were obtained using the Veeco NanoScope IIIa atomic force microscope (AFM). The fluorescence emission and excitation spectra and 3D fluorescence data were obtained by the HITACHI F-7000 fluorescence spectrophotometer. X-ray photoelectron spectroscopy (XPS) was performed via the Thermo VG ESCALAB 250 X-ray photo-electron spectrometer using Al Kα X-rays as the excitation source. The Fourier transform infrared (FTIR) spectra were obtained by the Nicolet 605 XB FT-IR spectrometer in the 4000–400 cm−1 range with a 2 cm−1 resolution. Raman measurements were carried out with the excitation of 633 nm using a confocal Raman microspectrometer (Renishaw, in Via-Reflex). Photoluminescence quantum yield (PLQY) was measured using the Nanolog FL3-2iHR infrared fluorescence spectrometer equipped with an integrating sphere. Temperature-dependent fluorescence spectra of CDs/LDH were obtained by the Craic 20/30 PV microspectrophotometer. Confocal microscopy images were obtained using the Leica TCS sp8 confocal laser scanning platform. The emission spectra and color coordinates of the WLED were determined by the Konica Minolta CS-2000 spectroradiometer.

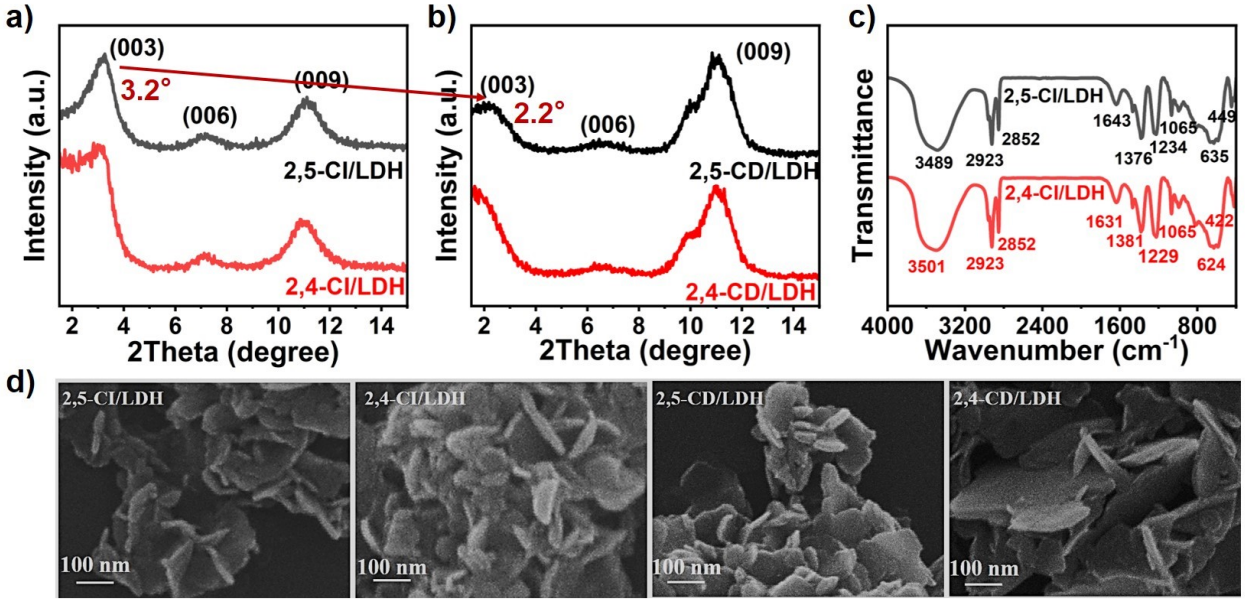

Fig. S1 (a)(b) XRD patterns (c) FT-IR spectra and (d) High-resolution SEM images of 2,5-CI/LDH, 2,4-CI/LDH, 2,5-CD/LDH and 2,4-CD/LDH.

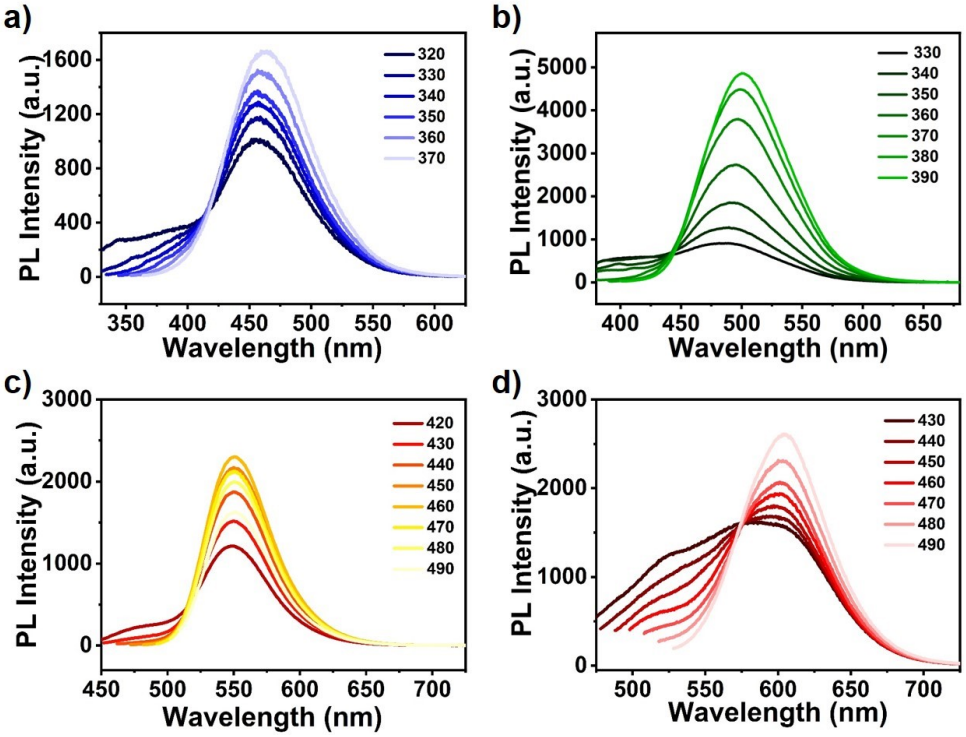

Fig. S2 PL emission spectra of (a)B-CS-CD, (b)G-UH-CD, (c)Y-CS-CD, (d)R-UH-CD.

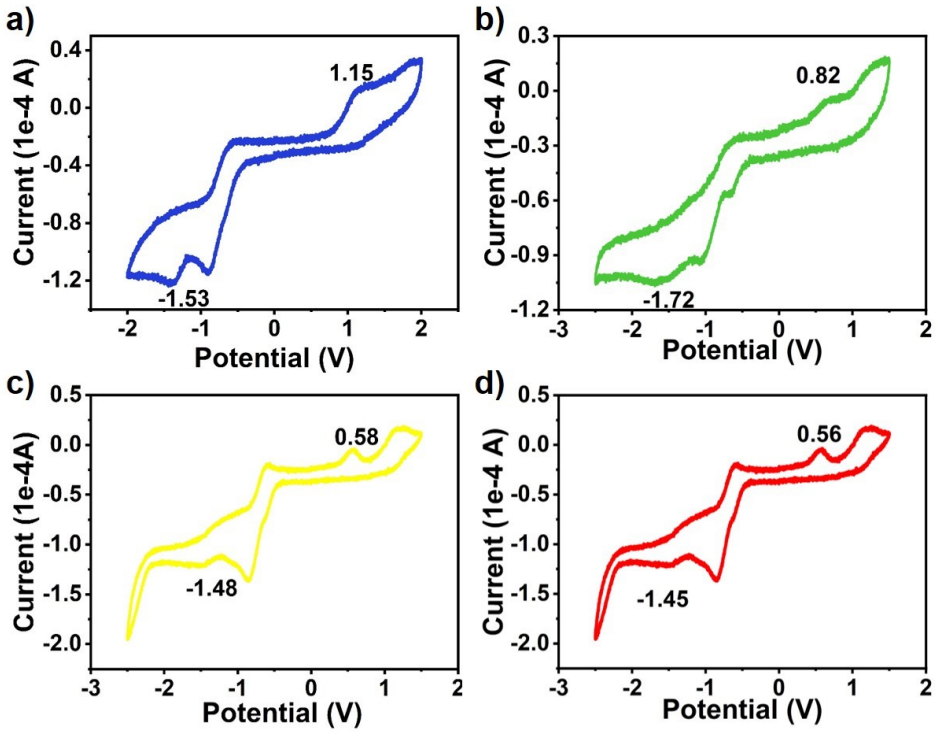

Fig. S3 Cyclic voltammogram curves of (a)B-CS-CD, (b)G-UH-CD, (c)Y-CS-CD, (d)R-UH-CD.

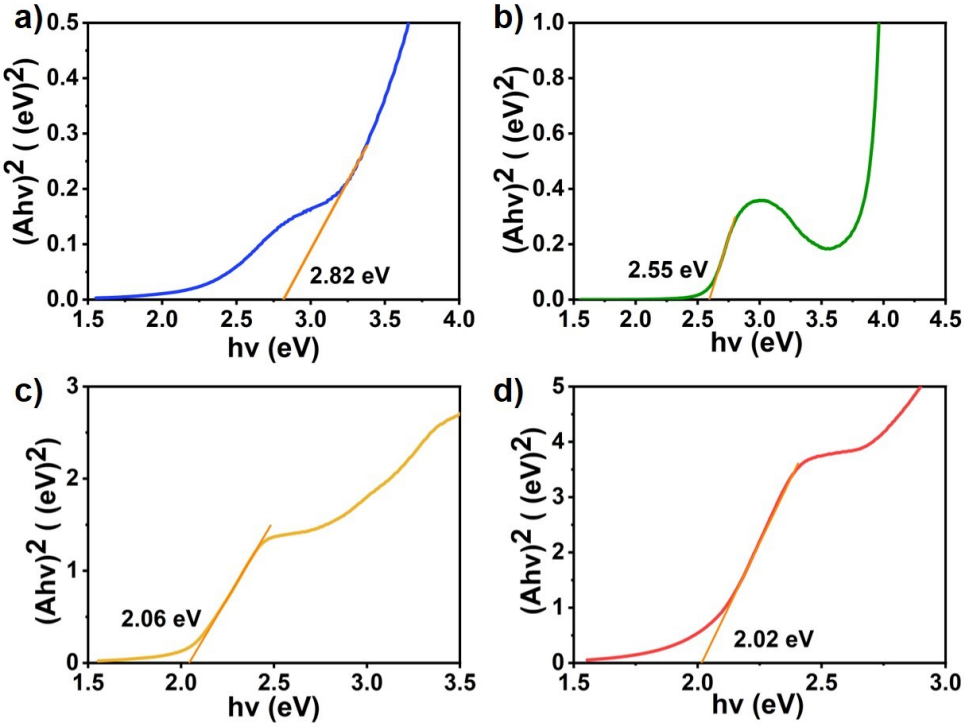

Fig. S4 UV-vis absorption threshold of (a)B-CS-CD, (b)G-UH-CD, (c)Y-CS-CD, (d)R-UH-CD.

Table S1. Average fluorescence lifetime of B-CS-CD, G-UH-CD, Y-CS-CD, R-UH-CD

Samples	B-CS-CD	G-UH-CD	Y-CS-CD	R-UH-CD
τ_1/ns	2.47	4.86	0.77	1.07
A_1/%	49.99	51.47	21.5	70.32
τ_2/ns	7.29	9.97	3.2	3.54
A_2/%	50.01	48.53	78.5	29.68
$\tau_{(avg)}$/ns	4.88	7.34	2.68	1.80
$\chi 2$	1.181	1.141	1.403	1.335

Table S2. Absolute photoluminescence quantum yield of B-CS-CD, G-UH-CD, Y-CS-CD, R-UH-CD

Samples	B-CS-CD	G-UH-CD	Y-CS-CD	R-UH-CD
QY/%	6.90	6.89	2.67	1.09

Table S3 The synthesis and fluorescent properties of recent reported multicolor CDs

Synthetic method	Fluorescence color	Emission wavelength (nm)	PLQY (%)	Refs.
Hydrothermal	Blue, Green, Red	492, 523, 601	13.1, 11.2, 9.8	S3
Solvothermal	Blue, Yellow-Green, Red	370, 440, 580	53.69, 54.88, 58.79	S4
Hydrothermal	Violet, Green, Orange	382, 516, 594	8.4, 9.3, 8.3	S5
Hydrothermal	Blue, Green, Orange	360, 530, 600	27.3, 18.4, 16.2	S6
Microwave	Blue, Green, Yellow, Orange, Red	445, 508, 546, 605, 635	48.2, 26.0, 18.5, 13.7, 5.7	S7
Solvothermal	Blue, Green, Red	460, 510, 605	62.79, 44.65, 20.88	S8

Solvothermal	Blue, Green, Red	410, 540, 646	0.80, 3.4, 16.6	S9
Solvothermal	Blue, Yellow, Red	440, 530, 620	29.17, 7.78, 6.80	S10
Microwave	Blue, Green, Red	405, 530, 600	12.0, 35.0, 8.0	S11
Solvothermal	Green, Yellow, Orange	535, 571, 602	56.0, 47.0, 34.0	S12
Hydrothermal	Green, Orange, Red	490, 600, 630	-, -, 14.0	S13
Solvothermal	Blue, Green, Yellow, Red	490, 530, 570, 605	32.3, 26.8, 22.6, 13.5	S14

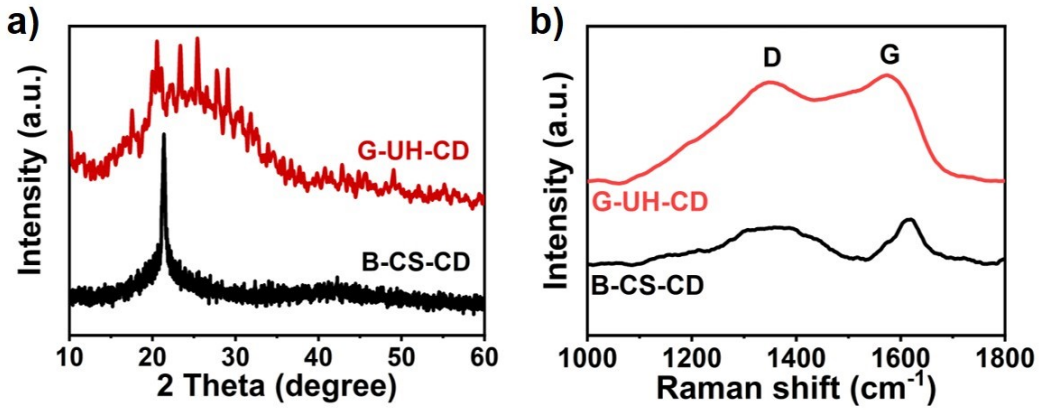

Fig. S5 (a) XRD of B-CS-CD, G-UH-CD, (b) Raman of B-CS-CD, G-UH-CD.

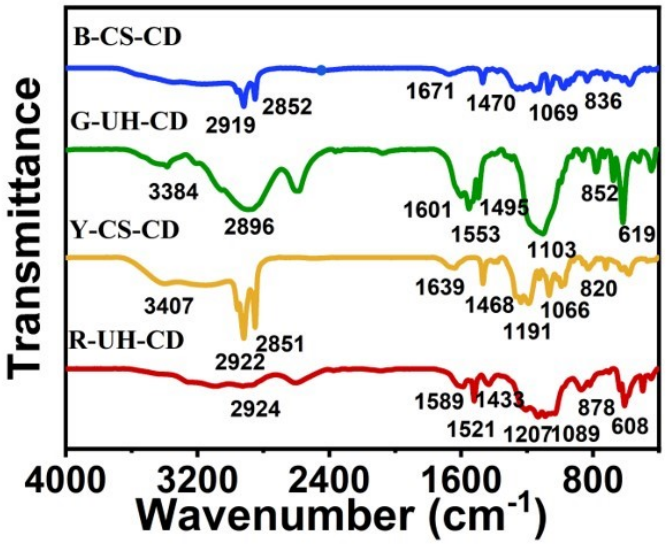

Fig. S6 FT-IR spectra of B-CS-CD, G-UH-CD, Y-CS-CD, R-UH-CD

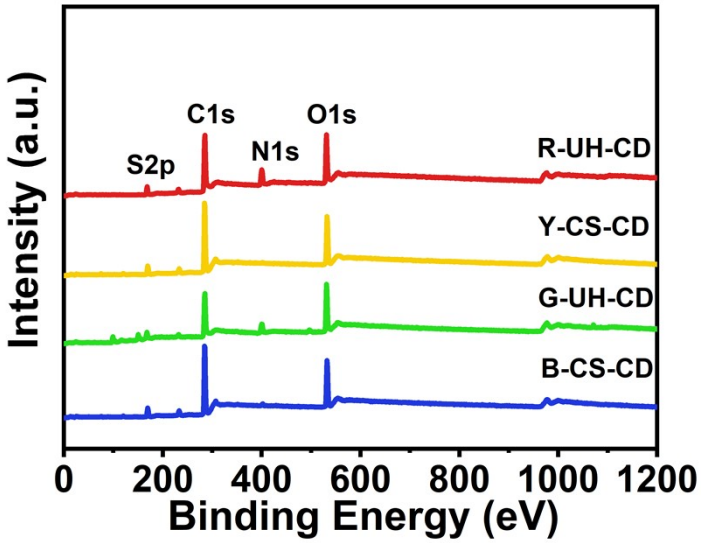

Fig. S7 XPS full spectrum of B-CS-CD, G-UH-CD, Y-CS-CD, R-UH-CD

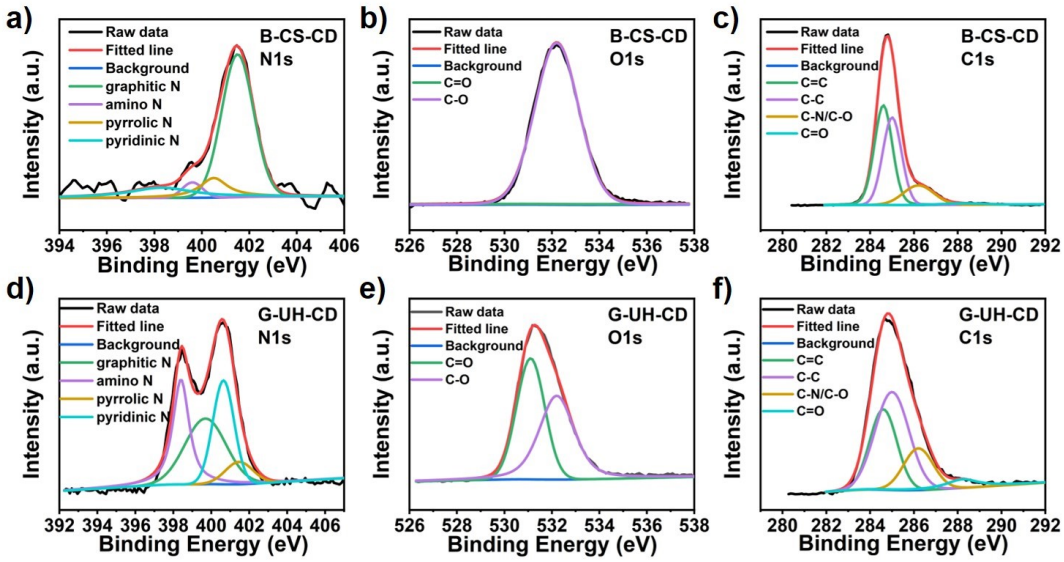

Fig. S8 The N1s, O1s and C1s high-resolution XPS spectra of B-CS-CD (a, b, c).and G-UH-CD (d, e, f)

Table S4. XPS data analyses of the C1s spectra of B-CS-CD, G-UH-CD, Y-CS-CD, R-UH-CD

Samples	C=C	C-C	C-N/C-O	C=O
B-CS-CD	44.59%	40.04%	14.34%	1.04%
G-UH-CD	31.49%	49.22%	16.78%	2.51%
Y-CS-CD	46.36%	36.84%	15.08%	1.72%
R-UH-CD	32.35%	44.66%	20.52%	2.48%

Table S5. XPS data analyses of the O1s spectra of B-CS-CD, G-UH-CD, Y-CS-CD, R-UH-CD

Samples	C=O	C-O
B-CS-CD	14.24%	85.76%
G-UH-CD	49.33%	50.67%
Y-CS-CD	1.55%	98.45%
R-UH-CD	59.36%	40.64%

Table S6. XPS data analyses of the N1s spectra of B-CS-CD, G-UH-CD, Y-CS-CD, R-UH-CD

Samples	Graphite N	Amino N	Pyrrolic N	Pyridine N
B-CS-CD	68.21%	4.64%	12.07%	15.08%
G-UH-CD	7.80%	34.15%	27.96%	30.09%
Y-CS-CD	63.65%	1.20%	34.45%	0.69%
R-UH-CD	5.24%	27.84%	47.78%	19.13%

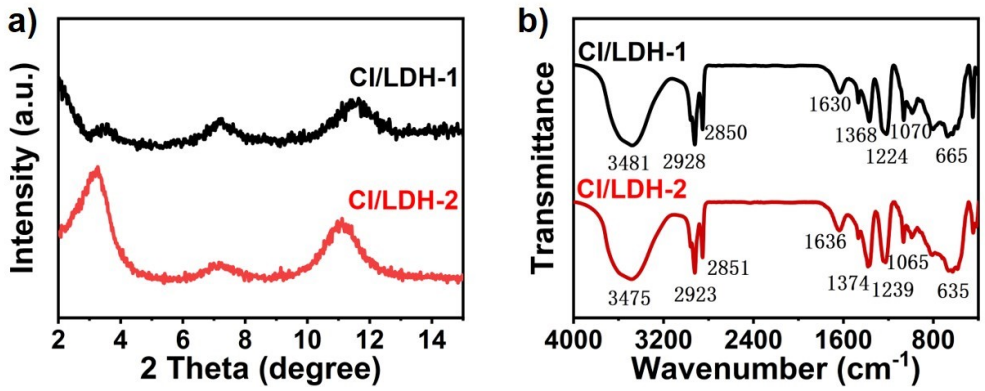

Fig. S9 (a) XRD patterns (b) FT-IR spectra of CI/LDH-1, CI/LDH-2.

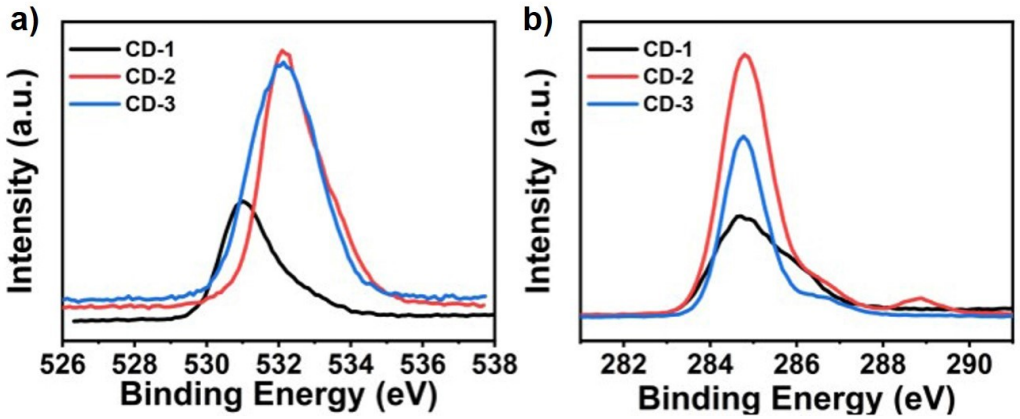

Fig. S10 The (a) O1s, (b) C1s XPS spectra of CD-1, CD-2 and CD-3.

References

S1 A. S. Bookin and V. A. Drits, Polytype Diversity of the Hydrotalcite-Like Minerals I. Possible Polytypes and their Diffraction Features, Clays Clay Miner., 1993, 41, 551-557.

S2 C. L. Brooks, Computer simulation of liquids, J. Solution Chem., 1989, 18, 99-99.

S3 S. S. H. Liao, X. Long, Y. S. Ma, S. G. Wu and J. Y. Wang, Synthesis of multicolor fluorescent carbon dots from zanthoxylum bungeanum and their application in fluorescent anti-counterfeiting ink, J. Photochem. Photobiol., A, 2023, 445, 115066.

S4 Q. Zeng, H. Qi, T. Jing, J. Li, S. Shen, H. Zhao and Y. Gao, Solvent-Engineered Strategy Synthesis of Multicolor Fluorescent Carbon Dots for Advanced Solid-State Lighting Applications, ACS Photonics, 2024, 11, 5128-5137.

S5 R. Y. Dai, X. P. Chen, N. Ouyang and Y. P. Hu, A pH-controlled synthetic route to violet, green, and orange fluorescent carbon dots for multicolor light-emitting diodes, Chem. Eng. J., 2022, 431,134172.

S6 J. Jia, W. Lu, S. Cui, C. Dong and S. Shuang, Synthesis of multicolor luminescent adjustable carbon dots and their application in anti-counterfeiting, Mater. Today Chem., 2022, 25, 100972.

S7 J. Wang, J. Zheng, Y. Yang, X. Liu, J. Qiu and Y. Tian, Tunable full-color solid-state fluorescent carbon dots for light emitting diodes, Carbon, 2022, 190, 22-31.

S8 X. R. Chen, X. Han, C. X. Zhang, X. Ou, X. L. Liu, J. H. Zhang, W. Liu, A. J. Ragauskas, X. P. Song and Z. Y. Zhang, Synthesis of Red, Green, and Blue Carbon Quantum Dots and Construction of Multicolor Cellulose-Based Light-Emitting Diodes, Small Struct., 2024, 5, 2300449.

S9 P. F. Li, S. S. Xue, L. Sun, X. B. Ma, W. N. Liu, L. An, Y. C. Liu, D. Qu and Z. C. Sun, Formation and Fluorescent Mechanism of Multiple Color Emissive Carbon Dots from o-Phenylenediamine, Small, 2024, 20, 2310563.

S10 S. S. Wei, B. Wang, H. Y. Zhang, C. Z. Wang, S. F. Cui, X. Y. Yin, C. Z. Jiang and G. Y. Sun, Portable smartphone platform based on tunable chiral fluorescent carbon dots for visual detection of L-Asp and L-Lys, Chem. Eng. J., 2023, 466, 143103.

S11 H. S. Shim, J. Choi, S. Jeong, S. Nam, J. Kim and J. K. Song, Fluorophore-Dependent Optical Properties of Multicolor Carbon Dots for Bioimaging and Optoelectronic Devices, ACS Appl. Nano Mater., 2023, 6, 17120-17129.

S12 J. Shen, X. J. Zheng, L. L. Lin, H. J. Xu and G. H. Xu, Reaction Time-Controlled Synthesis of Multicolor Carbon Dots for White Light-Emitting Diodes, ACS Appl. Nano Mater., 2023, DOI: 10.1021/acsanm.2c04764.

S13 Q. Bai, S. Ma, M. Yan, J. Wang, X. Wang and J. Ou, Preparation of pH-resistant multicolor thiol fluorescent carbon dot using cysteine and neutral red as precursors and its application in detection and adsorption of apigenin, Talanta, 2025, 286, 127520.

S14 G. H. Xu, J. Shen, L. G. Zhang, L. L. Lin, X. J. Zheng, X. C. Xu, P. F. Du and H. J. Xu, Synthesis of multicolor carbon dots at room temperature and in atmosphere toward energy-efficient preparation and LEDs application, Colloids Surf., A, 2024, 687, 133486.